**Communication**

# cMYC protein interactions and chromatin association in NUT carcinoma

Barry M. Zee[1,2#], Artyom A. Alekseyenko[1,2#], Anne E. Smolko[1,2], Mitzi I. Kuroda[1,2]*

*Corresponding author

#Equal contribution

[1]Div. of Genetics, Dept. of Medicine, Brigham and Women's Hospital, Boston, MA.

[2]Dept. of Genetics, Harvard Medical School, Boston, MA.

**Simple Summary:**

A longstanding goal in biology is to understand how protein interactions influence and reflect cellular disease states. MYC is a critical regulator of cellular proliferation that is mis-regulated in many cancers, including those with NUTM1-rearrangements featured in this issue. NUT carcinoma cells are dependent on MYC expression, which blocks differentiation. Using a small molecule inhibitor to induce differentiation of a NUTM1-rearranged patient cell line, we sought to understand how MYC protein interactions are affected by cellular status. When cells differentiate, we found MYC levels were globally diminished, yet the identities of its protein partners and genomic binding sites remained constant. During both growth and differentiation, MYC protein interacted with subunits of the NuA4 lysine acetyltransferase complex, similar to its associations in non-NUTM1 cell lines. Taken together, our results suggest that lysine acetyltransferase activities participate in multiple oncogenic steps in NUT carcinoma.

**Abstract:**

The oncogene c*MYC* (HGNC:7553) is a critical genomic target of the BRD4-NUT (B4N) protein that defines many of the NUTM1-rearrangement cancer subtypes in NUT carcinoma (NC). B4N interacts with the EP300 lysine acetyltransferase (KAT3B) to create hyperacetylated "megadomains" that activate downstream genes such as *cMYC*. However, it is less well understood how mis-regulation of cMYC in turn affects its protein interactions and target genes. The goals of this study are to define the protein and genomic interactions of cMYC in NC, and to test whether those change in response to B4N inactivation. We used CRISPR-Cas9 mediated knock-in of a BioTAP affinity tag to analyze cMYC protein expressed from its normal chromosomal context. This allowed us to adapt a crosslinking purification method termed BioTAP-XL to preserve cMYC integrity and chromatin association for genomic and mass spectrometry-based proteomic analyses. We found that cMYC interacts primarily with the NuA4 KAT5 lysine acetyltransferase complex and that the interactions were maintained despite a decrease in cMYC levels after JQ1 treatment. We conclude that a cascade of aberrant acetyltransferase activities, first via EP300 recruitment and then by KAT5 interaction with MYC, drive NC cell proliferation and blockade to differentiation.

**Keywords:** NUT carcinoma; cMYC; NuA4 acetyltransferase; KAT5; BioTAP-XL

43 **Graphical Abstract:**

44

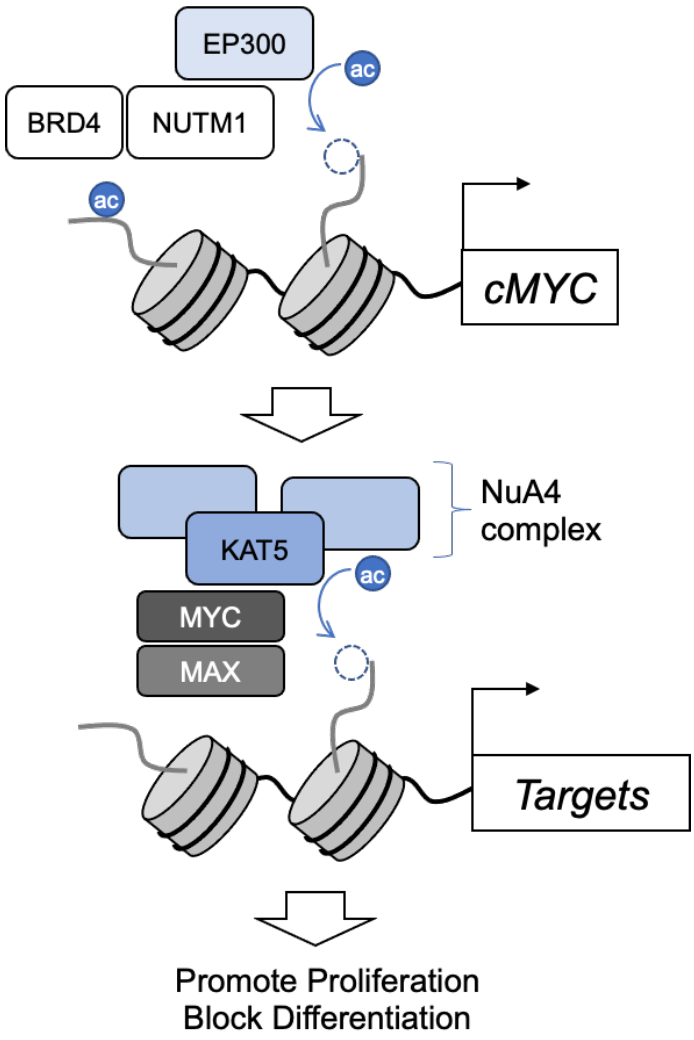


45

46

47

48 **1. Introduction**:

49 NUT-rearrangement cancers are a collection of aggressive and poorly-differentiated squamous cell
50 carcinomas whose unique molecular hallmark is somatic expression of *NUTM1* (HGNC:29919)[1].
51 Chromosomal rearrangements result in the otherwise germline-restricted *NUTM1* gene to be fused
52 downstream of a somatically expressed gene, most commonly *BRD4* (HGNC:13575) to generate
53 the fusion protein BRD4-NUT (B4N). At least two NC fusion proteins: B4N and ZNF532-NUT
54 (a fusion product with *ZNF532* (HGNC:30940)) have been shown to regulate expression of the
55 proto-oncogene *cMYC* (hereafter referred to as *MYC*). This is thought to occur through formation
56 of unusual hyperacetylated chromatin regions termed "megadomains" that can span several
57 megabases [2, 3]. Except for this common genomic region, the hundreds of other B4N and ZNF532-
58 NUT megadomains generally map to distinct regions. Treatment of NC patient cells in culture with
59 a small molecule, JQ1, that inhibits interaction of the BRD4 bromodomains with acetylated
60 lysines, leads to loss of megadomains, down-regulation of *MYC,* and differentiation of B4N cells
61 [2, 4]. The unique importance of *MYC* was revealed in studies where induced *MYC* transgene
62 expression reversed the differentiation induction caused by B4N knockdown [5]. Furthermore, non-
63 B4N-dependent pathways such as *KLF4* (HGNC:6348) expression help maintain *MYC* levels in
64 cells resistant to JQ1 [6]. Thus, understanding the mechanism of action of MYC in NC cells should
65 provide valuable insights into this therapeutically intractable disease.

66

67 Much of what is understood about MYC stems from non-NC cells [7-10]. MYC regulates the
68 expression of critical enzymes involved in growth and metabolism, thereby affecting global RNA
69 and protein expression. However, the direct target specificity of MYC remains a subject of debate,
70 in part due to an incomplete picture of the relationship between binding and function. There are

several technical challenges with studying how MYC is assembled with other factors. First, the MYC protein has a relatively short half-life of approximately 30 minutes, a result of ubiquitin-dependent and ubiquitin-independent pathways and of the even shorter (10 minute) half-life of *MYC* RNA itself [11-14]. Second, expression of the *MYC* gene depends on many long-range distal regulatory elements [15]. These challenges necessitate the ability to inactivate multiple cellular degradation machinery components and the ability to preserve the complex transcriptional regulatory circuits of the *MYC* locus. Here, we applied our previously published technique, BioTAP-XL [3, 16], to characterize the MYC protein and genomic interactions in NC and non-NC cells. We found that MYC interacts with subunits of the NuA4 acetytransferase complex in both cell types [17], and that MYC interactions in NC cells are largely maintained when JQ1 treatment reduces overall MYC levels, suggesting that protein complex assembly is independent of differentiation status. These results support models in which chromatin acetylation, especially of NuA4, plays a central role in the biological function of MYC [18, 19].

86 **2. Materials and Methods:**

87 *2.1 Generation of N-BioTAP-cMYC NC797 cells using CRISPR/Cas9*

88 To generate N-BioTAP and N-ProteinA (PrA) cMYC fusions in NC797 cells [20], the following
89 DNA fragments: pAVV-MCS-NheI-5'cMyc_BamHI-ATG-loxP-Blasti-P2A-loxP-PrA-Bio-
90 3'cMyc and pAAV-5'-cMYC-ATG-LoxP-Blasti-P2A-loxP-PrA-3'-cMYC respectively, were
91 synthesized as gBlock gene fragments (Integrated DNA Technologies, **Datafile S1**) and
92 introduced into the NheI/BamHI restriction sites of pAAV-MCS2 by Gibson assembly (New
93 England Biolabs). N-BioTAP and N-PrA cassettes targeted the first ATG of the *MYC* gene. The
94 pAAV-nEFCas9 (Addgene, plasmid 87115) was used to express Cas9, and the pAAV-tagBFP U6-
95 gRNA expression vector was used to express a gRNA targeting the start codon of cMYC: gRNA-
96 cMYC-start (**Table 1**). Recombinant AAV2 was packaged in HEK293T cells using pHelper and
97 pRC2-mi342 plasmids (Takara, Catalog #632608). Three days after transfection, cells were
98 harvested and AAV2 was isolated using AAVpro Extraction Solution (Takara, Catalog #6235).
99 Two million NC797 cells were infected with 30ul of each adeno-associated virus (AAV2).
100 Following 1 week of culture post-AAV infection, cells were selected with 7.5ug/ml Blasticidin
101 (Invitrogen**).** Surviving cells were re-plated and single-cell clones were isolated and expanded, and
102 genotyping PCR and sequencing were performed to check for proper integration of the BioTAP or
103 PrA cassette in the c-MYC locus. We recovered both heterozygous and homozygous clones.
104 Homozygosity of the cassette insertion was determined by absence of the wildtype PCR fragment
105 (1033bp) and presence of the larger PCR fragment (2083bp) with the following PCR primers:
106 Genom-Myc(1S) and Genom-Myc(1A) (**Table 1**). Next, we validated the presence of the correctly
107 sized tagged MYC protein and absence of wild type MYC by Western blot probed with a c-MYC
108 antibody (Rabbit mAb, Cell Signalling Technology, Cat# 5605). We selected homozygous clone

109 number 2 (for N-BioTAP-cMYC) and clone number 4 (for N-PrA-cMYC) for Cre-dependent
110 cassette excision experiments.
111
112 **Table 1. Sequences of oligonucleotides used in paper.**

| Name | Sequence (5′ to 3′) |
|---|---|
| gRNA-cMYC-start | GACGTTGAGGGGCATCGTCGC |
| Genom-Myc(1S) | GAGTGGGAACAGCCGCAG |
| Genom_Myc(1A) | CAGGTACAAGCTGGAGGTGG |

113
114 Next, the recombinant pAAV-CRE plasmid was packaged in HEK293T cells using pHelper and
115 pRC2-mi342 plasmids (Takara, Catalog #632608). Cells were harvested three days after
116 transfection and AAV2 was isolated using AAVpro Extraction Solution (Takara, Catalog #6235).
117 Two million 797 cells with homozygous insertions (clones 2 or 4) were infected with 30ul of each
118 adeno-associated CRE virus (AAV2). Following one week of culture post-AAV infection, cells
119 were re-plated, single-cell clones were isolated and expanded, and genotyping PCR and
120 sequencing were performed to check for absence of the drug resistance cassette in the c-MYC
121 locus. We selected clone number 2-7 (for N-BioTAP-cMYC) and clone number 4-6 (for N-PrA-
122 cMYC) to proceed with LC-MS and ChIP-seq experiments.
123
124 *2.2 Generation of inducible N and C-BioTAP-cMYC expressing HEK293T cells*
125 We used lentiviral transduction to generate stable HEK293T cell lines [2] carrying cMYC
126 constructs with the BioTAP tag at either the N or the C terminus to induce transcription of these
127 clones from the CMV/2xtetO promoter for genetic complementation experiments. To make N- and
128 C-terminal BioTAP constructs, we used the Gateway recombination system to introduce the
129 following Myc ORF clone HsCD00039771 in pDONR221from the CCSB Human ORFeome

130 Collection into pHAGE-TRE-DEST-NBioTAP (Addgene #53568) and pHAGE-TRE-DEST-
131 CBioTAP lentiviral vectors (Addgene #53569). Stable 293T-Trex-cell lines containing each
132 transgene were generated by lentiviral transduction in the presence of 8µg/mL polybrene, followed
133 by selection with 2µg/mL puromycin dihydrochloride (Sigma #P8833) as described previously [21].
134 To induce transcription of the cDNA clones from the CMV/2xtetO promoter we added
135 doxycycline (1µg/mL) to the medium for 48 hours.
136
137 *2.3 Proteomic analysis of cMYC interactions using BioTAP-XL*
138 All cell lines were cultured as monolayers in DMEM (Invitrogen) supplemented with 1x Penicillin
139 Streptomycin (Hyclone, South Logan, UT), 1x Glutamax (Gibco), and 10% (v/v) Fetal bovine
140 serum (FBS) (Hyclone). For JQ1 treatment, 500uM of JQ1 (gift from Dr. C.A. French) was added
141 to NC797 cells for various durations before harvesting for Western Blot analysis. The 12 hour
142 timepoint was ultimately chosen for BioTAP-XL experiments.
143
144 Our primary experiments were performed with 2-7 N-BioTAP-cMYC (clone 2-7). (2.0 × 10^9)
145 grown as monolayer cultures in 150-mm dishes. 100 plates total were used for BioTAP-XL
146 purification. The main steps of the BioTAP-XL procedure were as previously described [21]. For
147 single-step BioTAP-XL, proteins enriched by IgG-agarose beads were eluted and processed with
148 Agencourt AMPure-XP magnetic beads (Beckman Coulter) as previously described [22]. In brief,
149 fifty micrograms of eluted proteins were acidified and diluted with acetonitrile prior to binding by
150 magnetic beads. SDS was removed with ethanol and acetonitrile washes, and proteins were
151 digested with overnight trypsin incubation, yielding peptides for desalting and LC-MS analysis.
152 LC-MS acquisition and analyses were performed as previously described [3].

153

154 *2.3 Genomic analysis of cMYC binding*

155 ChIP-seq analysis was performed in parallel with proteomic analyses as previously described [16].
156 Raw fastq files were aligned to the human genome (hg38) using bowtie2.3.4.3 with default
157 settings [23]. Duplicate reads were then removed with samtools1.14 [24]. Peak calling was
158 performed on DMSO treated samples with HOMER4.9 using the findPeaks command [25].
159 HOMER annotatePeaks.pl was used to assign peaks to genomic regions. Deeptools3.0.2 was
160 used to generate bigwig files, enrichment profiles, and heatmaps [26]. Bigwig files were
161 normalized to 1x genome coverage. For heatmaps and enrichment profiles, MYC signal was
162 normalized to its corresponding input and enrichment was shown as $\log_2$(IP/input). Differential
163 peak analysis was performed with the DiffBind package in RStudio using default settings:
164 (http://bioconductor.org/packages/release/bioc/vignettes/DiffBind/inst/doc/DiffBind.pdf).
165 Datasets can be obtained from the NCBI GEO database (accession# GSE201033).

166

167 **3. Results:**

168 **3.1 Background on Affinity Approach**

169 To address the poor stability of MYC during conventional biochemical extraction and the risk of
170 losing key interactions during DNA removal, we applied a crosslinking approach termed BioTAP-
171 XL for MYC complex purification in NC797 cells, an NC line, and in HEK293 cells, a non-NC
172 line for comparison. The BioTAP affinity tag itself is composed of the Z domain from
173 *Staphylococcal* protein A and a biotinylation target domain from *Propionibacterium*
174 transcarboxylase. After generating a cell line that expresses the BioTAP-tagged bait, the BioTAP-
175 XL workflow involves three steps: 1) formaldehyde to inactivate cellular enzymes and to crosslink

176 proximal protein and nucleic acid interactions, 2) sonication to solubilize the crosslinked
177 chromatin pellet, and 3) enrichment of the tagged bait using tandem ProteinA and streptavidin
178 pulldowns combined with stringent washes to reduce nonspecific interactions. This approach has
179 successfully characterized the proteomic and genomic interactions of B4N, wild-type BRD4,
180 ZNF532-NUT, wild-type ZNF532, and other proteins [3].
181
182 **3.2 Proteomic profiling**
183 We next characterized the protein interactions of N-BioTAP-MYC in NC797 cells. Using a
184 CRISPR-Cas9 mediated knock-in approach, we successfully inserted the BioTAP affinity tag into
185 both copies of the endogenous *cMYC* gene in NC797 cells (see Methods, **Figure 1**). A critical
186 concern with interpreting affinity tag results is whether the tagged protein preserves the functions
187 of the non-tagged protein. In NC models such as NC797 cells, B4N regulates transcription of the
188 *MYC* gene, and NC797 cells are dependent on functional MYC expression [1, 2, 4, 5]. That we could
189 create viable homozygous knock-in NC797 cell lines expressing only BioTAP- or ProteinA-tagged
190 MYC strongly suggests that neither epitope tag interferes with normal MYC function, thus
191 enabling our biochemical and genomic interrogation of MYC using the BioTAP-XL procedure.
192

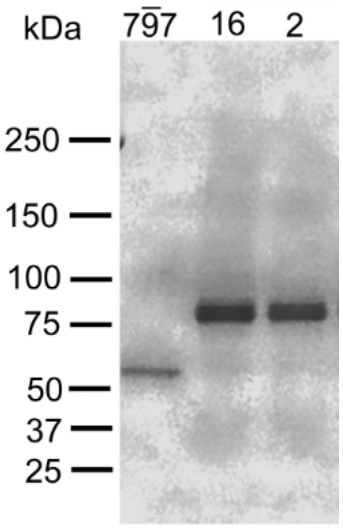


193

194 **Figure 1.** Western blot of NC797 cells carrying homozygous knock-in alleles of BioTAP-tagged
195 MYC probed with anti-MYC (D84C12 Rabbit mAb, Cell Signalling Technologies). The untagged
196 size of MYC in unedited NC797 cells is ~57 Kd, (lane 1). The size of N-BioTAP-MYC is ~80
197 Kd, seen in Clones 16 and 2 (lanes 2 and 3). Clone 2 was used for subsequent experiments.

198

199 We performed BioTAP-XL to enrich for MYC containing protein complexes and used liquid
200 chromatography-mass spectrometry (LC-MS) to sequence the peptides resulting from trypsin
201 digestion of the enriched complexes. MYC protein interactions were identified as the proteins with
202 the greatest fold enrichment in total peptides identified in the pulldown compared to the input
203 sample (**Datafile S2**). As expected, we recovered both MYC and its partner MAX as among the
204 top twenty-three most enriched proteins (corresponding to approximately the top one to two
205 percent). Beyond MYC and MAX, eleven of the most enriched proteins are related to chromatin
206 function. In particular, eight are components of the NuA4 histone acetyltransferase complex [17, 27]
207 (**Figure 2**). The enriched components include DMAP1 (HGNC:18291), EP400 (HGNC:11958),
208 EPC1 (HGNC:19876), EPC2 (HGNC:24543), KAT5 (HGNC:5275), MBTD1 (HGNC:19866),
209 TRRAP (HGNC:12347), and YEATS4 (HGNC:24859).

A

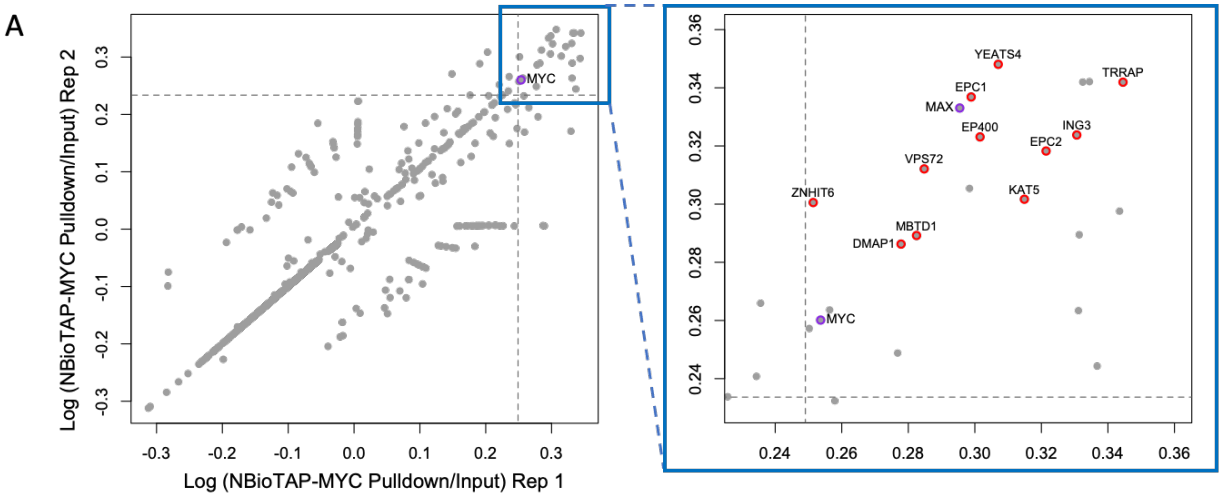


B

| | | | | MYC BioTAP | | MYC PrA Vehicle | | MYC PrA JQ1 | | |
|---|---|---|---|---|---|---|---|---|---|---|
| Name | MolWt | Input | JQ1 input | Rep #1 | Rep #2 | Rep #1 | Rep #2 | Rep #1 | Rep #2 | No Bait IgG |
| MYC | 50.53 | 0 | 0 | 3 | 3 | 7 | 8 | 3 | 6 | 0 |
| MAX | 18.26 | 0 | 0 | 3 | 4 | 7 | 9 | 6 | 7 | 0 |
| DMAP1 | 52.96 | 2 | 2 | 9 | 9 | 9 | 8 | 5 | 6 | 0 |
| EP400 | 343.28 | 8 | 7 | 58 | 66 | 53 | 46 | 35 | 29 | 0 |
| EPC1 | 93.41 | 0 | 0 | 7 | 10 | 4 | 7 | 2 | 4 | 0 |
| EPC2 | 91.04 | 0 | 0 | 9 | 8 | 10 | 8 | 6 | 7 | 0 |
| ING3 | 46.71 | 0 | 0 | 7 | 6 | 6 | 7 | 5 | 4 | 0 |
| KAT5 | 61.76 | 1 | 0 | 10 | 8 | 4 | 6 | 1 | 3 | 0 |
| MBTD1 | 70.5 | 0 | 0 | 5 | 5 | 3 | 2 | 2 | 3 | 0 |
| TRRAP | 437.32 | 9 | 8 | 106 | 95 | 87 | 85 | 52 | 79 | 0 |
| VPS72 | 41.82 | 0 | 1 | 4 | 5 | 4 | 4 | 2 | 3 | 0 |
| YEATS4 | 26.48 | 1 | 0 | 6 | 8 | 2 | 3 | 2 | 2 | 0 |
| ZNHIT6 | 53.88 | 0 | 0 | 3 | 5 | 1 | 1 | 0 | 1 | 0 |

**Figure 2.** Characterization of MYC protein interactions in NC797 cells.

(a) Scatterplots depicting enrichment of proteins from N-terminally tagged MYC using BioTAP-XL workflow in NC797 cells compared to non-enriched input. Each gray dot represents an individually identified protein, where its position is a measure of enrichment efficiency based on the number of total peptides identified in pulldown compared to input and normalized to the molecular weight of the protein from two technical replicates. The dashed gray lines denote the 98$^{th}$ percentile of enrichment. The right plot is a zoomed in region of the most enriched proteins in the left plot from replicate experiments. (b) Number of total peptides mapping to each protein from a given pulldown experiment.

221

222 To test whether the NuA4 interaction would change upon B4N inactivation and the resulting
223 cellular differentiation, we performed affinity enrichment of MYC after cells were treated with the
224 bromodomain inhibitor JQ1. We knew from prior experience that the amount of MYC bait protein
225 expression after inactivation of B4N would be significantly decreased, which might be insufficient
226 for a full tandem affinity purification. Therefore we modified our approach to utilize a single rather
227 than dual tag, utilizing NC797 clones in which the endogenous gene had only the ProteinA portion
228 of the affinity tag (PrA-MYC). Consistent with B4N directly regulating the endogenous *MYC*
229 locus, treatment of NC797 cells with JQ1 reduced levels of PrA-MYC in a time-dependent manner
230 (**Figure 3**). Interestingly, despite choosing a 12 hour timepoint that corresponded to a five-fold
231 reduction in PrA-MYC levels, we found the NuA4 complex interactions with MYC were largely
232 preserved after affinity enrichment (**Figure 2B**). To test whether recovery of NuA4 components is
233 due to non-specific capture of the proteins by the IgG agarose beads, we performed a parallel
234 pulldown with NC797 cells expressing no tagged bait. We observed no recovery of peptides from
235 MYC or NuA4 components (**Figure 2B**).

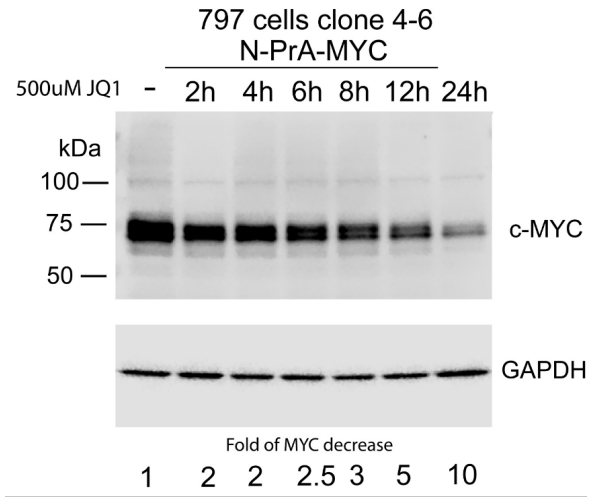


**Figure 3**. Effect of JQ1 treatment on MYC protein expression. Levels of MYC protein in N-PrA-cMyc-NC797 cells were assayed by Western blot, following different durations of 500uM JQ1 treatment, with approximate fold change in MYC levels provided below the plot compared to no treatment control.

243

244 Finally, to test whether the NuA4 complex interaction was NC-cell dependent, we performed the
245 BioTAP-XL experiment in the non-NC cell line HEK293-TREx. Similar to NC797 cells, we found
246 enrichment of NuA4 components with an inducibly expressed MYC-BioTAP bait in HEK293-
247 TREx cells (**Datafile S3**). Collectively, our results suggest that in NC797 patient cells the most
248 significant protein interactions of MYC besides MAX are members of the NuA4 acetyltransferase
249 complex. These interactions are maintained during differentiation induced by JQ1 treatment.
250

251 **3.3 Genomic profiling**

252 In parallel with the proteomic analyses, we mapped the genomic occupancy of PrA-MYC in
253 NC797 cells following JQ1 or DMSO treatment, to determine if its set of target genes changed as
254 its levels decreased. Differential binding analysis resulted in 2,238 regions with significantly
255 altered MYC binding (FDR < 0.05) (**Figure 4A,B**). Consistent with the decrease in MYC levels,
256 a majority of MYC-bound regions showed decreased occupancy (n=2,234). Significantly
257 downregulated regions were located at promoters (25%, n=555/2,234), introns (40%,
258 n=900/2,234), and intergenic regions (28%, n=623/2,234) (**Figure 4C)**. However, while MYC
259 occupancy was diminished, the identities of MYC binding sites were not globally changed by
260 JQ1 treatment (**Figure 4B,D**). Our comparison of proliferating and differentiating NC cells
261 suggests that MYC-dependent changes in cell state generally occur without alteration of key
262 MYC protein interactions or MYC binding sites.
263
264

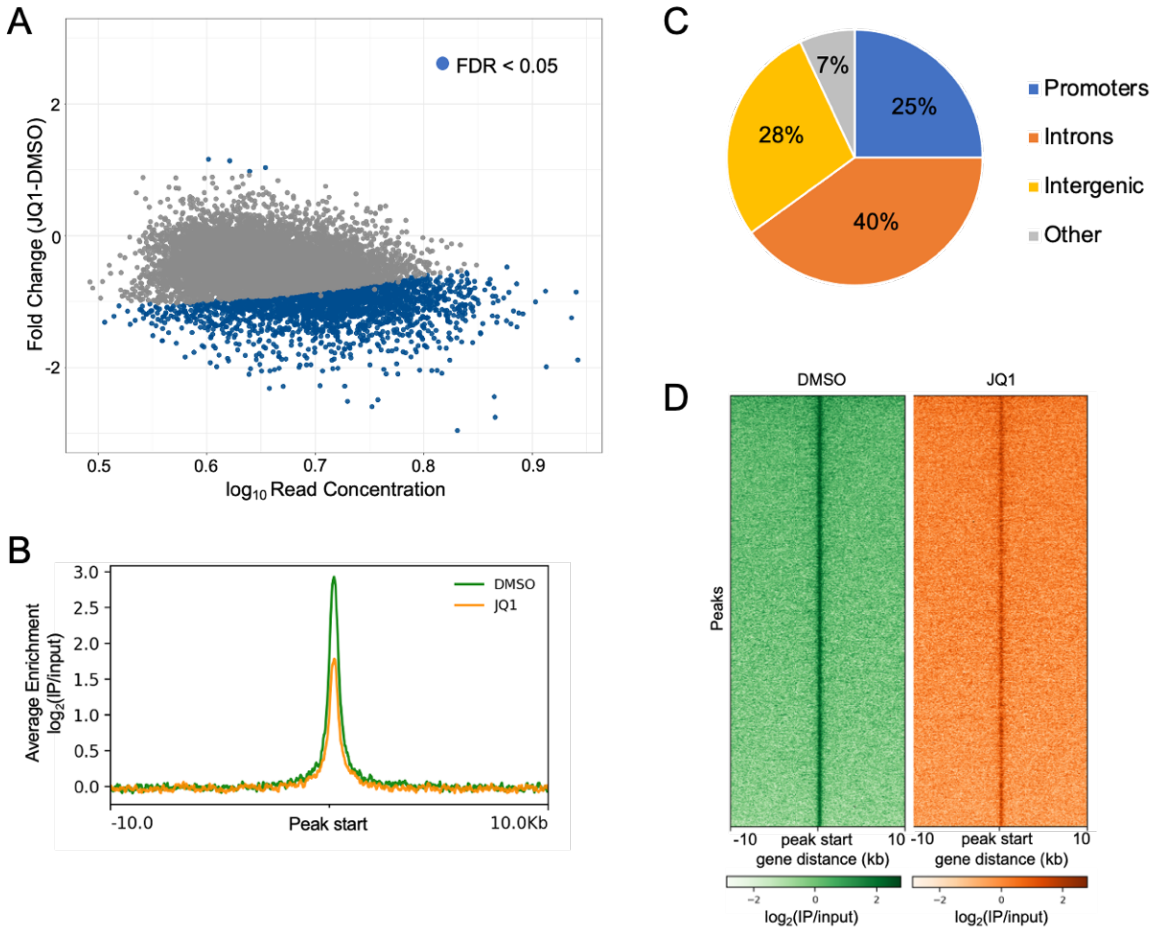


**Figure 4.** Effect of JQ1 on MYC genomic binding.

(a.) MA plot of MYC differential binding after JQ1 treatment. Each point represents a 400bp MYC-bound regions. Blue points indicate significantly altered regions (FDR < 0.05). The x-axis depicts the $\log_{10}$ of the average read concentration across all samples. The y-axis indicates the fold change after JQ1 treatment. (b.) Enrichment profile plotting the average signal of significantly decreased MYC-bound regions in DMSO and JQ1 treated samples. One representative replicate is shown. (c.) Pie chart depicting the percentage of significantly decreased MYC-bound regions mapped to the specified genomic regions. (d.) Heatmap of MYC enrichment at significantly decreased MYC-bound regions in DMSO and JQ1 treated samples. One representative replicate is shown.

276 **4. Discussion:**

277 To characterize MYC protein partners in NC797 cells, we applied a crosslinking affinity pulldown
278 method. We took this approach because, historically, MYC complexes have been difficult to
279 purify. Our data suggest significant interactions between MYC and NuA4 complex components.
280 The canonical NuA4 complex is comprised of the catalytic subunit KAT5, also known as TIP60,
281 and at least four non-catalytic subunits: EPC1, TRAAP, BAF53, DMAP1. Our results are
282 consistent with the links between MYC and histone acetyltransferase activity that were discovered
283 in some of the earliest studies of MYC function [18, 28-32], and more recent proteomic analyses using
284 targeted biotinylation [27] or BioID [33] to identify protein interactors in mouse and human cell lines,
285 respectively. Our datasets and methods should be useful in further study of MYC and downstream
286 targets specifically in NC cells. Furthermore, demonstrations that MYC is dependent on
287 acetyltransferases for its function suggest potential therapeutic options to what is generally
288 considered an undruggable oncoprotein [19, 34]. If specific inhibitors of KAT5 can be developed,
289 they might synergize with JQ1 in the potential future treatment of NC.

290

291 **5. Conclusion:**

292 MYC is a central player in a majority of cancers, yet understanding its regulation, targeting, and
293 mode of action are important unsolved problems. When we initiated this study, we knew that the
294 B4N oncogenic fusion attracted the p300 acetyltransferase to drive oncogenesis, with the Myc
295 gene as a critical target [1]. Since MYC function in NC cells is reversible by the JQ1 small molecule
296 BET bromodomain inhibitor, we saw this as an opportunity to compare MYC interactions in the
297 same cells under oncogenic and differentiating conditions. While we did not find a difference in
298 protein interactions or gene targeting in the distinct growth states, we confirmed a close association

between MYC and the NuA4 acetyltransferase in NC cells. We propose that future analysis of MYC transcriptional regulation in NUT carcinoma, and likely other cancers, should prioritize how MYC recruits KAT complexes to modify the chromatin of its many gene targets.

**Supplementary Materials:**

The following supporting information can be downloaded at: www.mdpi.com/xxx/s1:

Datafile S1: DNA sequences used to create NC797 cells with N-terminal fusions of the BioTAP- or Protein A-epitope tags to the endogenous cMYC coding region

Datafile S2: Total peptide counts of NC797 proteomic results

Datafile S3: Total peptide counts of HEK293T proteomic results

**Author Contributions:**

Conceptualization, AAA and MIK; methodology, validation, formal analysis, investigation, BMZ and AAA; resources, data curation, BMZ and AES; writing – original draft preparation BMZ and AAA; writing – review and editing, BMZ and MIK; visualization, BMZ, AAA, AES; supervision, project administration, funding acquisition, MIK. All authors have read and agreed to the published version of the manuscript.

**Funding:**

This research was funded by the National Institutes of Health, grant number R35 GM126944 to MIK. AES is supported by an American Cancer Society postdoctoral fellowship 721690.

## Data Availability Statement

Proteomic data sets can be found at Harvard Dataverse (https://doi.org/10.7910/DVN/IFKRBT).

Genomic data sets can be found at NCBI GEO database (accession# GSE201033).


## Acknowledgments

We thank Dr. C.A. French for introducing us to NC research, and Dr. J.L. Makofske for initial work on this project. We thank Ross Tomaino (Taplin Mass Spectrometry Facility, Harvard Medical School) for expert help with analyzing the proteomics samples. We thank Drs. T. Martin and S.J. Elledge for the pAAV-tagBFP U6-gRNA expression vector. Finally, we thank H.J. Kang for helpful assistance with data submission.


## Conflicts of Interest

The authors declare no conflict of interest.

## References


1. French, C. A., NUT Carcinoma: Clinicopathologic features, pathogenesis, and treatment. *Pathol Int* **2018,** *68* (11), 583-595.
2. Alekseyenko, A. A.; Walsh, E. M.; Wang, X.; Grayson, A. R.; Hsi, P. T.; Kharchenko, P. V.; Kuroda, M. I.; French, C. A., The oncogenic BRD4-NUT chromatin regulator drives aberrant transcription within large topological domains. *Genes Dev* **2015,** *29* (14), 1507-23.
3. Alekseyenko, A. A.; Walsh, E. M.; Zee, B. M.; Pakozdi, T.; Hsi, P.; Lemieux, M. E.; Dal Cin, P.; Ince, T. A.; Kharchenko, P. V.; Kuroda, M. I.; French, C. A., Ectopic protein interactions within BRD4-chromatin complexes drive oncogenic megadomain formation in NUT midline carcinoma. *Proc Natl Acad Sci U S A* **2017,** *114* (21), E4184-E4192.
4. Filippakopoulos, P.; Qi, J.; Picaud, S.; Shen, Y.; Smith, W. B.; Fedorov, O.; Morse, E. M.; Keates, T.; Hickman, T. T.; Felletar, I.; Philpott, M.; Munro, S.; McKeown, M. R.; Wang, Y.; Christie, A. L.; West, N.; Cameron, M. J.; Schwartz, B.; Heightman, T. D.; La Thangue, N.; French, C. A.; Wiest, O.; Kung, A. L.; Knapp, S.; Bradner, J. E., Selective inhibition of BET bromodomains. *Nature* **2010,** *468* (7327), 1067-73.
5. Grayson, A. R.; Walsh, E. M.; Cameron, M. J.; Godec, J.; Ashworth, T.; Ambrose, J. M.; Aserlind, A. B.; Wang, H.; Evan, G.; Kluk, M. J.; Bradner, J. E.; Aster, J. C.; French, C.

353 A., MYC, a downstream target of BRD-NUT, is necessary and sufficient for the blockade of
354 differentiation in NUT midline carcinoma. *Oncogene* **2014,** *33* (13), 1736-1742.
355 6. Liao, S.; Maertens, O.; Cichowski, K.; Elledge, S. J., Genetic modifiers of the BRD4-NUT
356 dependency of NUT midline carcinoma uncovers a synergism between BETis and CDK4/6is.
357 *Genes Dev* **2018,** *32* (17-18), 1188-1200.
358 7. Meyer, N.; Penn, L. Z., Reflecting on 25 years with MYC. *Nature reviews. Cancer* **2008,** *8*
359 (12), 976-90.
360 8. Dang, C. V., MYC on the path to cancer. *Cell* **2012,** *149* (1), 22-35.
361 9. Kress, T. R.; Sabo, A.; Amati, B., MYC: connecting selective transcriptional control to global
362 RNA production. *Nature reviews. Cancer* **2015,** *15* (10), 593-607.
363 10. Muhar, M.; Ebert, A.; Neumann, T.; Umkehrer, C.; Jude, J.; Wieshofer, C.; Rescheneder,
364 P.; Lipp, J. J.; Herzog, V. A.; Reichholf, B.; Cisneros, D. A.; Hoffmann, T.; Schlapansky,
365 M. F.; Bhat, P.; von Haeseler, A.; Kocher, T.; Obenauf, A. C.; Popow, J.; Ameres, S. L.;
366 Zuber, J., SLAM-seq defines direct gene-regulatory functions of the BRD4-MYC axis. *Science*
367 **2018,** *360* (6390), 800-805.
368 11. Hann, S. R.; Eisenman, R. N., Proteins encoded by the human c-myc oncogene: differential
369 expression in neoplastic cells. *Mol Cell Biol* **1984,** *4* (11), 2486-97.
370 12. Hickman, K. A.; Hariharan, S.; De Melo, J.; Ylanko, J.; Lustig, L. C.; Penn, L. Z.; Andrews,
371 D. W., Image-Based Analysis of Protein Stability. *Cytometry A* **2020,** *97* (4), 363-377.
372 13. Murai, N.; Murakami, Y.; Tajima, A.; Matsufuji, S., Novel ubiquitin-independent nucleolar
373 c-Myc degradation pathway mediated by antizyme 2. *Sci Rep* **2018,** *8* (1), 3005.
374 14. Dani, C.; Blanchard, J. M.; Piechaczyk, M.; El Sabouty, S.; Marty, L.; Jeanteur, P., Extreme
375 instability of myc mRNA in normal and transformed human cells. *Proc Natl Acad Sci U S A*
376 **1984,** *81* (22), 7046-50.
377 15. Cole, M. D., MYC association with cancer risk and a new model of MYC-mediated repression.
378 *Cold Spring Harb Perspect Med* **2014,** *4* (7), a014316.
379 16. Alekseyenko, A. A.; McElroy, K. A.; Kang, H.; Zee, B. M.; Kharchenko, P. V.; Kuroda, M.
380 I., BioTAP-XL: Cross-linking/Tandem Affinity Purification to Study DNA Targets, RNA, and
381 Protein Components of Chromatin-Associated Complexes. *Curr Protoc Mol Biol* **2015,** *109*,
382 21 30 1-21 30 32.
383 17. Doyon, Y.; Cote, J., The highly conserved and multifunctional NuA4 HAT complex. *Curr*
384 *Opin Genet Dev* **2004,** *14* (2), 147-54.
385 18. Frank, S. R.; Parisi, T.; Taubert, S.; Fernandez, P.; Fuchs, M.; Chan, H. M.; Livingston, D.
386 M.; Amati, B., MYC recruits the TIP60 histone acetyltransferase complex to chromatin. *EMBO*
387 *Rep* **2003,** *4* (6), 575-80.
388 19. Numata, A.; Kwok, H. S.; Zhou, Q. L.; Li, J.; Tirado-Magallanes, R.; Angarica, V. E.;
389 Hannah, R.; Park, J.; Wang, C. Q.; Krishnan, V.; Rajagopalan, D.; Zhang, Y.; Zhou, S.;
390 Welner, R. S.; Osato, M.; Jha, S.; Bohlander, S. K.; Gottgens, B.; Yang, H.; Benoukraf, T.;
391 Lough, J. W.; Bararia, D.; Tenen, D. G., Lysine acetyltransferase Tip60 is required for
392 hematopoietic stem cell maintenance. *Blood* **2020,** *136* (15), 1735-1747.
393 20. Toretsky, J. A.; Jenson, J.; Sun, C. C.; Eskenazi, A. E.; Campbell, A.; Hunger, S. P.; Caires,
394 A.; Frantz, C.; Hill, J. L.; Stamberg, J., Translocation (11;15;19): a highly specific
395 chromosome rearrangement associated with poorly differentiated thymic carcinoma in young
396 patients. *Am J Clin Oncol* **2003,** *26* (3), 300-6.

21. Alekseyenko, A. A.; Gorchakov, A. A.; Kharchenko, P. V.; Kuroda, M. I., Reciprocal interactions of human C10orf12 and C17orf96 with PRC2 revealed by BioTAP-XL cross-linking and affinity purification. *Proc Natl Acad Sci U S A* **2014,** *111* (7), 2488-93.
22. Zee, B. M.; Alekseyenko, A. A.; McElroy, K. A.; Kuroda, M. I., Streamlined discovery of cross-linked chromatin complexes and associated histone modifications by mass spectrometry. *Proc Natl Acad Sci U S A* **2016,** *113* (7), 1784-9.
23. Langmead, B.; Salzberg, S. L., Fast gapped-read alignment with Bowtie 2. *Nat Methods* **2012,** *9* (4), 357-9.
24. Danecek, P.; Bonfield, J. K.; Liddle, J.; Marshall, J.; Ohan, V.; Pollard, M. O.; Whitwham, A.; Keane, T.; McCarthy, S. A.; Davies, R. M.; Li, H., Twelve years of SAMtools and BCFtools. *Gigascience* **2021,** *10* (2).
25. Heinz, S.; Benner, C.; Spann, N.; Bertolino, E.; Lin, Y. C.; Laslo, P.; Cheng, J. X.; Murre, C.; Singh, H.; Glass, C. K., Simple combinations of lineage-determining transcription factors prime cis-regulatory elements required for macrophage and B cell identities. *Mol Cell* **2010,** *38* (4), 576-89.
26. Ramirez, F.; Ryan, D. P.; Gruning, B.; Bhardwaj, V.; Kilpert, F.; Richter, A. S.; Heyne, S.; Dundar, F.; Manke, T., deepTools2: a next generation web server for deep-sequencing data analysis. *Nucleic Acids Res* **2016,** *44* (W1), W160-5.
27. Kim, J.; Woo, A. J.; Chu, J.; Snow, J. W.; Fujiwara, Y.; Kim, C. G.; Cantor, A. B.; Orkin, S. H., A Myc network accounts for similarities between embryonic stem and cancer cell transcription programs. *Cell* **2010,** *143* (2), 313-24.
28. McMahon, S. B.; Wood, M. A.; Cole, M. D., The essential cofactor TRRAP recruits the histone acetyltransferase hGCN5 to c-Myc. *Mol Cell Biol* **2000,** *20* (2), 556-62.
29. Bouchard, C.; Dittrich, O.; Kiermaier, A.; Dohmann, K.; Menkel, A.; Eilers, M.; Luscher, B., Regulation of cyclin D2 gene expression by the Myc/Max/Mad network: Myc-dependent TRRAP recruitment and histone acetylation at the cyclin D2 promoter. *Genes Dev* **2001,** *15* (16), 2042-7.
30. Frank, S. R.; Schroeder, M.; Fernandez, P.; Taubert, S.; Amati, B., Binding of c-Myc to chromatin mediates mitogen-induced acetylation of histone H4 and gene activation. *Genes Dev* **2001,** *15* (16), 2069-82.
31. Fernandez, P. C.; Frank, S. R.; Wang, L.; Schroeder, M.; Liu, S.; Greene, J.; Cocito, A.; Amati, B., Genomic targets of the human c-Myc protein. *Genes Dev* **2003,** *17* (9), 1115-29.
32. Knoepfler, P. S.; Zhang, X. Y.; Cheng, P. F.; Gafken, P. R.; McMahon, S. B.; Eisenman, R. N., Myc influences global chromatin structure. *Embo J* **2006,** *25* (12), 2723-34.
33. Dingar, D.; Kalkat, M.; Chan, P. K.; Srikumar, T.; Bailey, S. D.; Tu, W. B.; Coyaud, E.; Ponzielli, R.; Kolyar, M.; Jurisica, I.; Huang, A.; Lupien, M.; Penn, L. Z.; Raught, B., BioID identifies novel c-MYC interacting partners in cultured cells and xenograft tumors. *J Proteomics* **2015,** *118*, 95-111.
34. Mustachio, L. M.; Roszik, J.; Farria, A.; Dent, S. Y. R., Targeting the SAGA and ATAC Transcriptional Coactivator Complexes in MYC-Driven Cancers. *Cancer Res* **2020,** *80* (10), 1905-1911.